Available online at www.sciencedirect.com
SCIENCE DIRECT®
Thermochimica Acta 412 (2004) 55–62
thermochimica acta
www.elsevier.com/locate/tca

Non-isothermal studies for the decomposition course of CdC_2O_4–ZnC_2O_4 mixture in air

M.A. Gabal*

Chemistry Department, Faculty of Science, Benha University, Benha, Egypt

Received 28 March 2003; received in revised form 27 August 2003; accepted 30 August 2003

Abstract

The thermal decomposition of cadmium–zinc oxalate (1:1 mol ratios) mixture in air was investigated by non-isothermal thermogravimetric analysis. Intermediates and the final products were characterized by X-ray diffraction and scanning electron microscopy techniques. TG showed that the mixture dehydrated in two steps and decomposed exothermically to CdO–ZnO mixture at 390 °C in a further two steps. The observed increase in the intensity of the X-ray diffraction lines by raising the calcination temperature from 400 to 800 °C is attributed to the grain growth of CdO–ZnO mixture as revealed from SEM experiments. The kinetics of the oxalate decomposition steps was performed using the various reaction interface models and differential techniques of computational analysis of non-isothermal data. The activation parameters, calculated using the integral composite method, showed that the reactions were best described by the random nucleation model characteristic of solid state nucleation growth mechanism. The results of activation parameters for the different decomposition steps are compared and discussed.

Keywords: CdC_2O_4; ZnC_2O_4; DTA-TG; SEM; Kinetics; Oxalates

1. Introduction

The thermal decomposition of metal oxalates is occasionally adopted as a means of preparing metals or metal oxides possessing pores, lattice imperfections and other characteristics necessary for their function as reactive solids [1]. Much researches [2] has been done on the structure, properties and thermal decomposition behaviors of metal oxalates and a considerable amount of information on the kinetics of the thermal dehydration and decomposition of them have been reported [3]. The combination of transition metal oxides may results in the modification of their thermal behavior, geometric structure and electronic properties that lead to changes in their catalytic functions [4]. Thus, the different synthesis methods of the mixed metal oxides and their characterization have been the subject of many numerous investigations.

The physico-chemical properties as well as the reactivity towards the reduction with hydrogen of CuO–Cr_2O_3 mixed oxides prepared by the thermal decomposition of basic metal carbonate precipitates have been investigated by means of various techniques [5]. Mucka and Pavek [6] tested the catalytic activity of the two-component oxide catalyst CdO–ZnO prepared from the thermal decomposition of nitrate precursors by means of hydrogen peroxide decomposition in a water solution. Giullermo et al. [7] studied the electrical and optical properties of a mixed thin film oxides of cadmium and zinc with different compositions prepared by spray pyrolysis deposition on a glass substrates.

The mixed metal oxalates [8]; $FeCu(OX)_2{\cdot}3H_2O$, $CoCu(OX)_2{\cdot}3H_2O$ and $NiCu(OX)_2{\cdot}3.5H_2O$ ($OX = C_2O_4^{-}$) have been prepared by coprecipitation technique and their thermal behaviors in nitrogen and oxygen have been examined using thermogravimetry (TG), thermomagnetometry (TM), differential scanning calorimetry (DSC) and evolved gas analysis (EGA). In a previous paper [9], the thermal decomposition processes taking place in the solid state mixed oxalates of (CuC_2O_4–$ZnC_2O_4{\cdot}2H_2O$, 1:1 mol ratios) was studied in air using differential thermal analysis thermogravimetry (DTA-TG), X-ray diffraction (XRD) and scanning electron microscopy (SEM) techniques. The kinetics of the oxalate decomposition steps were performed under non-isothermal conditions using different integral methods of analysis of dynamic data.

* Present address: Institute of Mechanical Engineering and Mechanics (IMVM), University of Karlsruhe, Geb. 30.70, Kaiser Street 12, Karlsruhe 76128, Germany. Tel.: +49-201-01048600; fax: +49-201-3222578.
E-mail address: mgabalabdo@yahoo.com (M.A. Gabal).

0040-6031/$ – see front matter © 2003 Elsevier B.V. All rights reserved.
doi:10.1016/j.tca.2003.08.025

The dynamic thermogravimetric analysis has been widely used as a tool to investigate the sample composition, the thermal stability as well as the kinetic data relating the chemical changes occur on heating [10]. In the present study, the thermogravimetry was used to study the kinetics of the thermal decomposition of $CdC_2O_4{\cdot}3H_2O$–$ZnC_2O_4{\cdot}2H_2O$ (1:1 mol ratios) mixture in air. The kinetic analysis of data were performed and considered with reference to the various theoretical model equations and integral methods of dynamic data analysis. The thermal decomposition course of the mixture was characterized using DTA-TG, XRD and SEM techniques.

2. Experimental

2.1. Materials

Pure metal oxalates were prepared by precipitation from aqueous solutions of analytical reagents $3CdSO_4{\cdot}8H_2O$ or $ZnCl_2{\cdot}2H_2O$ on the addition of hot oxalic acid solution. The physical mixture $CdC_2O_4{\cdot}3H_2O$–$ZnC_2O_4{\cdot}2H_2O$ (1:1 mol ratios) was prepared by the impregnation method. The appropriate mole ratios of the individual metal oxalates were grounded together in a porcelain mortar. During the vigorous stirring, drops of bi-distilled water were added to assure complete homogeneity. The wet oxalate mixture was dried at 60 °C for about 2 h.

On the basis of the thermal analysis results, the calcination products of the mixture were obtained by heating the mixture in static air at 340 °C for 15 min, at 400 °C for 1 h or at 800 °C for 2 h. Prior to the analysis, the calcinations products were kept dry over anhydrous calcium chloride in a desiccator.

2.2. Apparatus

Thermal analysis experiments including thermogravimetry (TG), differential thermogravimetry (DTG) and differential thermal analysis (DTA) were carried out using a Shimadzu DT-40 thermal analyzer. All the experiments were carried out in a dynamic (30 ml min^{-1}) atmosphere of air in order to prevent the accumulation of the gaseous products. Sample weights in the Pt-cell of 8–10 mg, were used in these experiments, to ensure linear heating rates and accurate temperature measurements. Highly sintered α-Al_2O_3 powder (Shimadzu) was used as the reference material for the DTA measurements. In the dynamic studies, the temperature was raised up to 400 °C at heating rates of 1, 2, 3 and 5 °C min^{-1}.

X-ray powder diffraction analysis of the solid decomposition products was carried out using a Philips PW 1710 diffractometer at ambient temperature using Ni-filtered Cu Kα radiation (λ = 1.5406 Å). For the identification purpose, the relative intensities (I/I_0) and the *d*-spacing (Å) were compared with standard diffraction patterns of the ASTM powder diffraction files [11].

SEM is performed using Jeol T 300 (Japan) scanning electron microscope operated at 15 keV. Mixtures were mounted separately on aluminum substrates evacuated to 10^{-3} Torr and precoated (20 and 5 min for each side of the four sides) in a sputter-coater with a thin uniform gold/palladium film to minimize charging in the electron beam. The applied voltage is 1.2–1.6 kV.

2.3. Data analysis

Kinetics parameters such as the activation energy (E) and the frequency factor (A) were calculated from the dynamic TG curves assuming the Diefallah's composite integral method based either on the modified Coats–Redfern equation (composite method I) or on Doyle's equation (composite method II) [9,12,13]. In the composite method I, the modified Coats–Redfern equation was rewritten in the form:

$$\ln\left[\frac{\beta g(\alpha)}{T^2}\right] = \ln\left(\frac{AR}{E}\right) - \frac{E}{RT} \quad (1)$$

where A is the frequency factor, E the energy of activation and $g(\alpha)$ the kinetic model function calculated for the fraction reacted (α) at temperature T and heating rate β. Table 1 shows the different kinetic model functions used in this work [9]. In the composite method II, Doyle's equation has been rewritten in the form:

$$\log g(\alpha)\beta = \left[\log\frac{AE}{R} - 2.315\right] - 0.4567\frac{E}{RT} \quad (2)$$

hence, the dependence of $\ln[\beta g(\alpha)/T^2]$ or $\log[g(\alpha)\beta]$, calculated for the different α-values at their respective β-values on $1/T$ must give rise to a single master straight line for the correct form of $g(\alpha)$. Generally, the results always show that [9,12,13] both the composite methods of analysis gave equivalent curves and nearly identical values for the calculated activation parameters. The composite method also

Table 1
Kinetic equations examined in this work

Reaction model	$g(\alpha)$	Symbol
One-dimensional diffusion	α^2	D_1
Two-dimensional diffusion	$\alpha + (1-\alpha)\ln(1-\alpha)$	D_2
Jander equation, three-dimensional diffusion	$[1-(1-\alpha)^{1/3}]^2$	D_3
Ginsling–Braunshtein equation, three-dimensional diffusion	$(1-2/3\alpha)-(1-\alpha)^{2/3}$	D_4
Two-dimensional phase boundary reaction	$[1-(1-\alpha)^{1/2}]$	R_2
Three-dimensional phase boundary reaction	$[1-(1-\alpha)^{1/3}]$	R_3
First order kinetic, Mampel unimolecular law	$[-\ln(1-\alpha)]$	F_1
Random nucleation: Avrami equation	$[-\ln(1-\alpha)]^{1/2}$	A_2
Random nucleation: Erofeev equation	$[-\ln(1-\alpha)]^{1/3}$	A_3
Exponential law	$\ln\alpha$	E_1

involves a model-fitting kinetic approach, since it does not assume a particular reaction model, but it allows the choice of the kinetic mechanism which best fits the data and gives the highest correlation coefficient.

The activation parameters were then calculated using two other integral methods: the Coats–Redfern method [14] and the Ozawa method [15] assuming the best fit kinetic model obtained from the composite method. The obtained activation parameters were then compared with those obtained according to the composite method and discussed.

3. Results and discussion

3.1. Thermal analysis

Fig. 1 shows the characteristic features of heating $CdC_2O_4{\cdot}3H_2O$–$ZnC_2O_4{\cdot}2H_2O$ (1:1 mol ratio) mixture in air atmosphere from the ambient temperature to 400 °C. It shows the DTA, TG and DTG curves that were measured at 5 °C min^{-1}. The TG curve shows four mass loss steps. The first two steps occurring at 65–140 °C and are accompanied by 11.5 and 8.5% mass loss, i.e. a total mass loss of 20.0% which is attributed to the complete dehydration of the mixture with the formation of anhydrous mixture (theoretical mass loss, 20.3%). From the theoretical mass loss, the first step can be attributed to the dehydration of $CdC_2O_4{\cdot}3H_2O$ and the second one is attributed to the dehydration of $ZnC_2O_4{\cdot}2H_2O$. Nagase et al. [16] showed that the dehydration temperature is a function of the size of metal ion and that it increases with the decrease in the radius of the metal ion. The ionic radius [17] of Cd(II) and Zn(II) ions are 0.97 and 0.76 Å, respectively. Thus, $CdC_2O_4{\cdot}3H_2O$ must be dehydrated at lower temperature than $ZnC_2O_4{\cdot}2H_2O$. The anhydrous mixture is thermally stable up to 290 °C after which a two consecutive mass loss steps were occurred in the temperature ranges 290–340 and 340–380 °C. These steps were associated by 16.5 and 16.7% mass loss due to the decomposition of CdC_2O_4 and ZnC_2O_4 in their mixture to CdO and ZnO (theoretical mass loss in both the steps is 16.2%), respectively. The total mass loss after complete decomposition was calculated to be 42.4% of the molecular mass of the reactants. From the above data, the temperatures equivalent to the theoretical mass losses can then be considered as the minimum temperatures which can be selected for the calcination process.

The DTG curve displays four broad peaks, which are closely correspond to the weight changes observed on the TG curves, with maximum rates of loss at about 92, 136, 326, and 366 °C, respectively.

The DTA curve reveals also four broad peaks maximized at 90 °C (endo), 132 °C (endo), 330 °C (exo) and 365 °C (exo), respectively. The two endothermic peaks are attributed to dehydration. Dollimore et al. [18,19] studied the thermal decomposition of ZnC_2O_4 and CdC_2O_4 in air and nitrogen atmospheres and found that the end product in case of ZnC_2O_4 to be ZnO in both atmospheres whereas in case of CdC_2O_4 the end product in nitrogen is Cd metal and in air is CdO. Thus the exothermic nature of the DTA peaks accompanying the first oxalate decomposition process (i.e. the decomposition process of CdC_2O_4) is attributed to the air oxidation of Cd metal to CdO, whereas the exothermic behavior of the second oxalate decomposition process (i.e. the decomposition process of ZnC_2O_4) is due to the catalytic oxidation reaction of CO as it forms to CO_2 on the surface of ZnO product.

The above thermal analysis results indicate that, $CdC_2O_4{\cdot}3H_2O$ and $ZnC_2O_4{\cdot}2H_2O$ decomposed in their mixture similarly to their individual metal oxalates [18,19]. This behavior is ascribed to the absence of any solid solution between the two metal oxalates and that each one behaves as it is present alone in the mixture. A similar behavior was obtained for the thermal decomposition reaction of CuC_2O_4–$ZnC_2O_4{\cdot}2H_2O$ mixture [9].

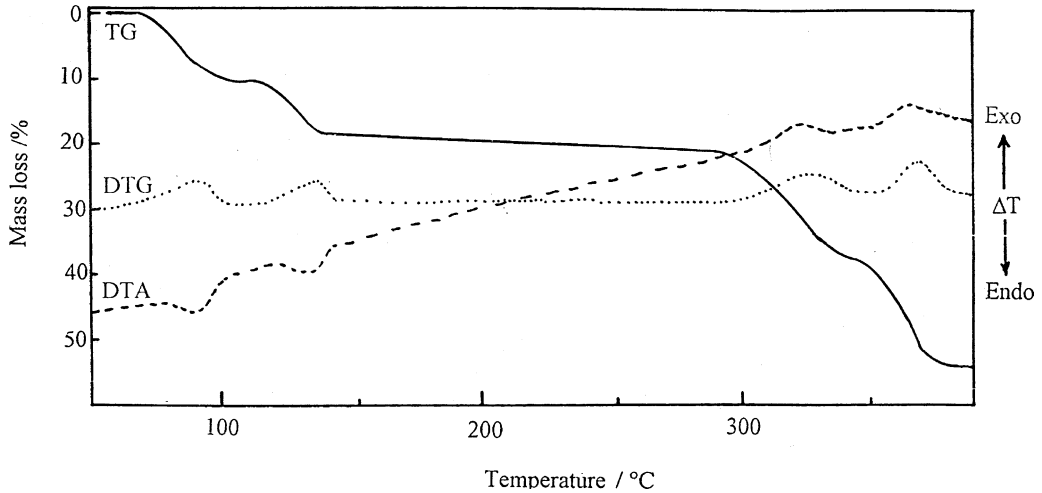

Fig. 1. DTA-TG curves of $CdC_2O_4{\cdot}3H_2O$–$ZnC_2O_4{\cdot}2H_2O$ (1:1 mol ratios) mixture in air at heating rate of 5 °C min^{-1}.

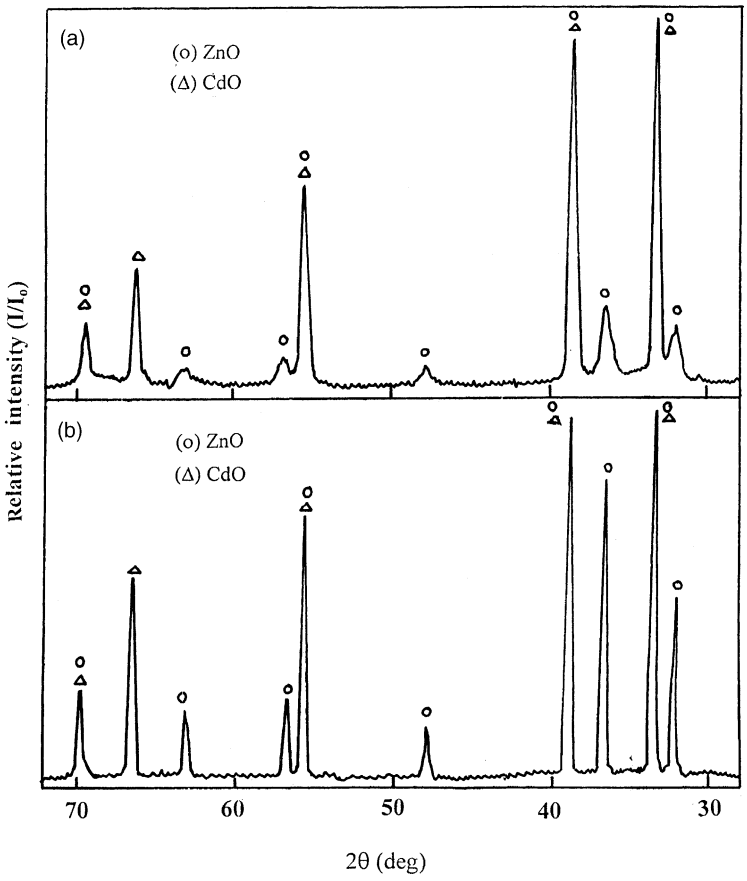

Fig. 2. Characteristic parts of XRD patterns of $CdC_2O_4{\cdot}3H_2O$–$ZnC_2O_4{\cdot}2H_2O$ (1:1 mol ratios) mixture calcined at different temperatures. Mixture calcined at (a) 400 °C and (b) 800 °C.

3.2. X-ray diffraction

The XRD diffraction pattern of the initial mixture matched the standard data compiled in the JCPDS data [11] no. 14–750 and 25–1029 for individual $CdC_2O_4{\cdot}3H_2O$ and $ZnC_2O_4{\cdot}2H_2O$, respectively. The XRD pattern of the decomposition products at 340 °C reveals the characteristic XRD lines for CdO (JCPDS no. 5–640). The presence of some XRD lines characteristic of hydrated zinc oxalate may be attributed to the hydration of the anhydrous zinc oxalate [20] formed at this decomposition stage.

Fig. 2 shows the characteristic X-ray diffraction patterns at ambient temperature for mixture calcined at 400 and 800 °C for the mixture calcined at 400 °C, the presence of the individual characteristic XRD lines (Fig. 2a) of both CdO and ZnO (JCPDS no. 5–640 and 21–1486, respectively) indicate the complete decomposition of the mixture without formation of any solid solution. The broadening of the XRD lines is attributed to the weak crystallinity of the decomposition products. Generally no solid solution was detected between the two metal oxides even by raising the calcination temperature to 800 °C. This was achieved by comparing the XRD patterns of the mixture calcined at 400 °C with that calcined at 800 °C (Fig. 2a and b), where the only difference is the increase in the intensities of the XRD lines. This behavior is ascribed to the sintering process. $(ZnO)_x(CdO)_{1-x}$ thin films of $(ZnO)_x(CdO)_{1-x}$ prepared by spray pyrolysis on a glass substrates [7] showed the presence of CdO XRD pattern for low zinc concentrations and a mixture of CdO (cubic) and ZnO (hexagonal) phases for the higher concentrations. The XRD pattern of this system shows also an increase in the crystallite sizes with annealing. A similar trend was also obtained for CuO–ZnO mixture prepared from CuC_2O_4–$ZnC_2O_4{\cdot}2H_2O$ (1:1 mol ratios) mixture [9].

3.3. Electron microscopy

Samples of the initial mixture as well as intermediate decomposition products formed at different temperatures were examined using scanning electron microscopy to characterize the textural changes that occurring during the decomposition reaction of the mixture. The parent mixture has very small individual crystallites (<0.5 μm) which make the textural features resolution difficult. The change in the particle size and shape throughout the decomposition process is shown in Fig. 3. The scanning electron micrograph of the mixture calcined at 340 °C (Fig. 3a) shows, in addition to the large irregularly shaped crystals of different sizes, aggregates of approximately spherical particles showing no regular or characteristic crystalline structures.

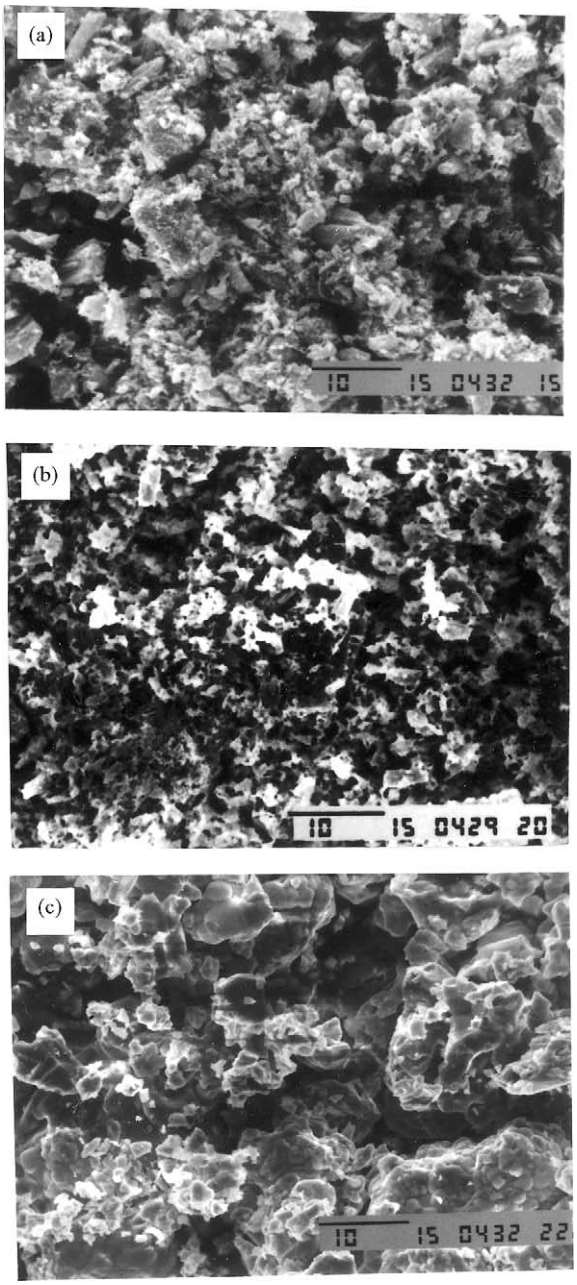

Fig. 3. Scanning electron micrograph showing the changes in texture and morphology that accompany the thermal decomposition of $CdC_2O_4{\cdot}3H_2O$–$ZnC_2O_4{\cdot}2H_2O$ (1:1 mol ratios) mixture in air. Mixture calcined at (a) 340 °C, (b) 400 °C and (c) 800 °C (scale bar 10 μm).

At this calcinations temperature the DTA-TG results show only the decomposition of CdC_2O_4 content into CdO while ZnC_2O_4 content remains undecomposed. The large crystals can be assigned to the undecomposed zinc oxalate while the particles aggregates can be ascribed to the decomposition of cadmium oxalate content into small and fine granules with roughening of the crystal surfaces. At 400 °C, the zinc oxalate content was decomposed, so, the micrograph obtained for the mixture at this temperature (Fig. 3b) shows the complete breaking into fine granules, with superficial roughening of the crystal edges, which provide evidence that the oxides formed at this stage are microcrystalline as previously suggested by XRD experiments. In the mixture calcined at 800 °C, these fine granules were coalesced into large aggregates of cubic crystals of different sizes (Fig. 3c).

3.4. Kinetic studies

The kinetics of the thermal decomposition in air of CdC_2O_4 to CdO (step III) and of ZnC_2O_4 to ZnO (step IV) in $CdC_2O_4{\cdot}3H_2O$–$ZnC_2O_4{\cdot}2H_2O$ (1:1 mol ratio) mixture were studied under non-isothermal conditions. Typical plots of weight changes from dynamic measurements at different constant heating rates versus decomposition temperature for these two steps are shown in Fig. 4. Kinetic analysis of data according to the composite method showed that the decomposition steps were best described by Avrami–Erofeev random nucleation equations (A_2 and A_3) characteristic of solid state nucleation growth mechanism, consistent with the textural changes that accompanying the decomposition as revealed by SEM experiments. The phase boundary controlled reaction equations (R_2 and R_3), in which an interface moves at constant velocity and nucleation occurs virtually instantaneously, gave also a satisfactory results. The other model equations give a less satisfactory fit of the data and the exponential law equation (E_1) gave the least fit. Table 2 lists the values of activation parameters, calculated according to the composite method based on the Doyle's equation (composite II method) assuming different heterogeneous solid state models, for the non-isothermal decomposition of CdC_2O_4 and ZnC_2O_4 in their mixture. Fig. 5 shows the typical results calculated by the composite method on the basis of the Doyle's equation assuming A_2 and E_1 models.

The activation parameters were also calculated on the basis of the Coats–Redfern and Ozawa methods assuming A_2 model (as revealed by the composite method). Then the calculation results according to the three computational methods were summarized in Table 3. The listed values for the activation parameters in case of the Coats–Redfern and the Ozawa methods are the average ones calculated at different heating rates (β) and fractional reaction (α) values, respectively.

Approximately constant E with α was obtained on plotting the calculated activation energy (E), estimated by the Ozawa method, versus the fractional reacted vales (α) for the two oxalate decomposition reactions (Fig. 6). As a result, this will enhance that the rate-limiting step is a single reaction step [9] in accordance with the single master straight line for all (α, β, T) values obtained at different heating rates estimated by the composite method (Fig. 5).

The results of data analysis using the different computational methods (Table 3) show a good agreement within experimental errors between the values of the calculated activation parameters. The data also shows that, the integral composite method of analysis gave the least standard deviation in the calculated experimental parameters. Generally,

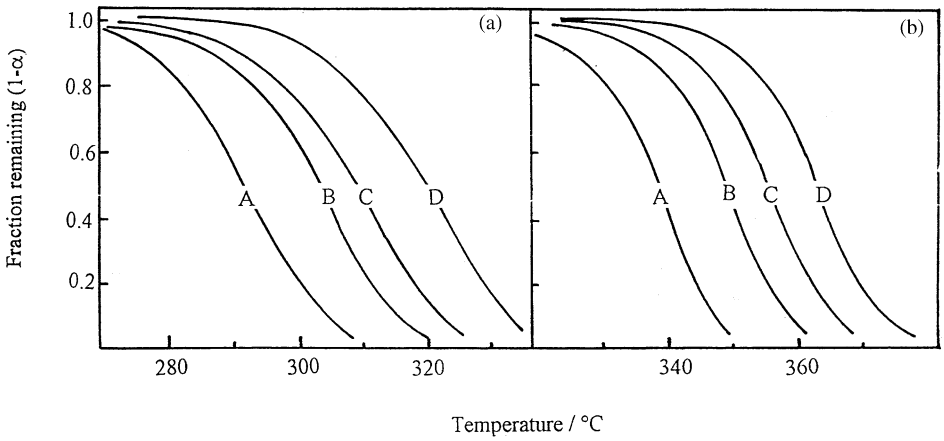

Fig. 4. Dynamic measurements for the thermal decomposition of $CdC_2O_4{\cdot}3H_2O$–$ZnC_2O_4{\cdot}2H_2O$ (1:1 mol ratios) mixture in air. (a) Decomposition of CdC_2O_4 to CdO and (b) ZnC_2O_4 to ZnO. Heating rate: curve A, 1 °C min^{-1}; curve B, 2 °C min^{-1}; curve C, 3 °C min^{-1} and curve D, 5 °C min^{-1}.

Table 2
Activation parameters of the non-isothermal decomposition in air of CdC_2O_4 and ZnC_2O_4 in their mixture, calculated according to the composite method II, assuming different kinetic models

Model	Decomposition of CdC_2O_4 (step III)			Decomposition of ZnC_2O_4 (step IV)		
	E (kJ mol^{-1})	log A (min^{-1})	r	E (kJ mol^{-1})	log A (min^{-1})	r
D_1	355 ± 21	30.8 ± 2.1	0.872	529 ± 35	30.0 ± 3.4	0.817
D_2	378 ± 23	32.8 ± 2.2	0.873	562 ± 44	30.0 ± 3.7	0.816
D_3	407 ± 25	35.0 ± 2.4	0.872	604 ± 47	30.0 ± 3.9	0.816
D_4	387 ± 24	33.1 ± 2.3	0.873	575 ± 45	30.0 ± 3.8	0.816
R_2	218 ± 8	18.3 ± 0.7	0.952	318 ± 15	25.4 ± 1.3	0.961
R_3	225 ± 8	18.8 ± 0.8	0.951	327 ± 16	26.1 ± 1.4	0.913
F_1	241 ± 9	20.9 ± 0.9	0.946	357 ± 18	28.5 ± 1.6	0.907
A_2	142 ± 2	11.9 ± 0.2	0.994	210 ± 3	16.6 ± 0.2	0.995
A_3	109 ± 4	8.9 ± 0.4	0.855	163 ± 3	12.7 ± 0.3	0.982
E_1	133 ± 25	13.3 ± 2.3	0.467	168 ± 38	15.2 ± 3.2	0.402

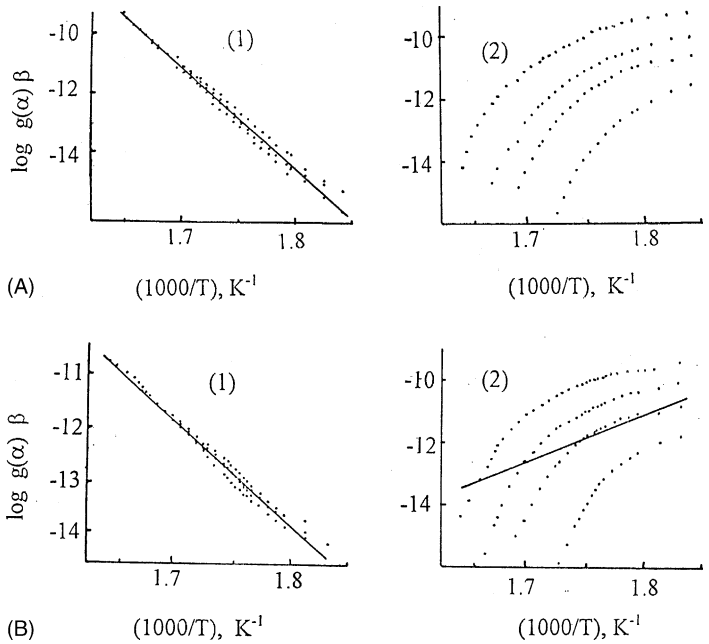

Fig. 5. Composite analysis of TG data for the non-isothermal decomposition in air of (A) CdC_2O_4 and (B) ZnC_2O_4 in their mixture based on Doyle's equation assuming: (1) A_2 model; (2) E_1 model.

Table 3
Activation parameters of the non-isothermal decomposition in air of CdC_2O_4 and ZnC_2O_4 in their mixture calculated according to A_2 model

Method of analysis	Decomposition of CdC_2O_4 (step III)		Decomposition of ZnC_2O_4 (step IV)	
	E (kJ mol^{-1})	log A (min^{-1})	E (kJ mol^{-1})	log A (min^{-1})
Composite II	142 ± 2	11.9 ± 0.2	210 ± 3	16.6 ± 0.2
Coats–Redfern	136 ± 10	11.3 ± 0.7	216 ± 16	17.2 ± 1.4
Ozawa	153 ± 4	12.9 ± 0.3	198 ± 5	15.6 ± 0.5

on comparing the activation energies obtained in Table 3 for the thermal decomposition of CdC_2O_4 and ZnC_2O_4 in their mixture it is obvious that the activation energy for the thermal decomposition of zinc oxalate is higher (about 30% more) than that needed for the thermal decomposition of cadmium oxalate. In addition, the DTA-TG results (Fig. 1) shows that the thermal stability of CdC_2O_4 is less than that of ZnC_2O_4.

In the oxalates of bivalent metals:

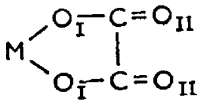

the extent to which the M–O_I bond is covalent depend on the electronegativity of the metal. Decomposition will occur when a temperature is reached at which the rupture of the M–O_I link is possible or at which the rupture of C–O_I bond occurs. For these oxalates which produce the metal in nitrogen the decomposition temperature represents the temperature at which the M–O_I link ruptured and will depend critically on the size and charge of the metal ion. Whereas in these decompositions where the oxide is produced in nitrogen the decomposition temperatures represents the energy required to break the C–O_I bond and this will depend less critically on the nature of cation. If the reaction proceeds by the rupture of the C–O_I bond, this would be followed by the rupture of the second M–O_I bond because the inability of the metal to accommodate two oxygen atoms.

The thermal decomposition of ZnC_2O_4 in air or nitrogen atmospheres results in the production of ZnO, whereas the thermal decomposition of CdC_2O_4 in nitrogen produces Cd metal, which in air is oxidized to CdO. Since the ionic radius [17] of Cd(II) is much higher than that of Zn(II), thus, based on the coulombic attraction the zinc will have a stronger M–O_I bond than that of cadmium. This would increase the energy needed to break the Zn–O bond, and thus increases the activation energy for the reaction. Dollimore and Griffths [18] also showed that, there is a decrease in the decomposition temperature with increase in the ionic radius of the metal ion. A decrease in the M–O_I bond strength would thus lead to a decrease in the decomposition temperature. Thus, the CdC_2O_4 will posses a lower decomposition temperature than ZnC_2O_4 as can be observed from the DTA-TG curves (Fig. 1).

In addition, the thermal stability of the metal oxalates decrease with the increase in the electron affinity of the metal ion. The oxidation–reduction potential measures the relative electron affinities of the metal ions forming oxalates, since Dq values of H_2O is near to that of $C_2O_4^-$ [21]. The reduction potential of cadmium ($E^0_{Cd^{2+}/Cd} = -0.403$ V) is higher than that of zinc ($E^0_{Zn^{2+}/Zn} = -0.763$ V), therefore, the

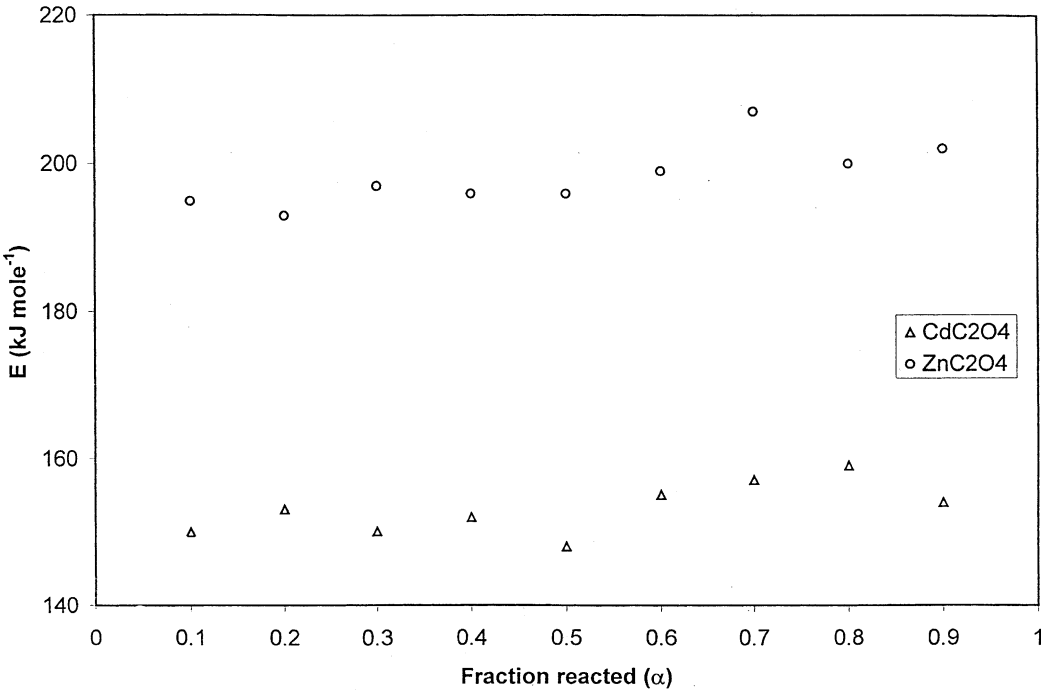

Fig. 6. Plots of the activation energies versus α calculated by Ozawa method for the thermal decomposition of CdC_2O_4 and ZnC_2O_4 in their mixture.

thermal stability of CdC_2O_4 is lower than that of ZnC_2O_4. The same effect was observed for central metal ions in potassium salts of metal oxalato complexes [21].

Moreover, the effect of the enthalpy of the reaction on the sample temperature and activation energy of the decomposition cannot be ignored [22,23]. The exothermicity of the CdC_2O_4 decomposition is more than the ZnC_2O_4 decomposition as evident from DTA curve (Fig. 1). This is due to the fact that the CdC_2O_4 decomposition in air is accompanied by the exothermic oxidation reaction of cadmium metal to CdO. The excessive heat transfer would allow ease rupture of the $M–O_I$ bond in the CdC_2O_4 than in the ZnC_2O_4.

4. Conclusions

DTA-TG experiments of $CdC_2O_4·3H_2O–ZnC_2O_4·2H_2O$ (1:1 mol ratio) mixture in air show that the mixture was completely decomposed to CdO–ZnO mixture through four well-defined steps. Intermediate decomposition products as well as the final products were characterized by X-ray diffraction and SEM techniques. XRD experiments show the absence of any formed solid solution even by raising the calcinations temperature to 800 °C. The increase in the intensity of the diffraction lines by raising the calcinations temperature from 400 to 800 °C is attributed to the grain growth of the decomposition products. SEM experiments confirmed this result as the fine granules obtained at 400 °C were coalesced into large aggregates of large crystals when calcined at 800 °C. Kinetic analysis of the data for the oxalate decomposition steps according to the integral composite method showed that the oxalate decomposition steps are best described by the Avrami–Erofeev equation characteristic of the solid state nucleation growth mechanism. The activation parameters were then calculated and discussed in view of the ionic radius and the electronegativity of the metal ions.

Acknowledgements

The author would like to thank Prof. Dr. A.A. El-Bellihi, Chemical Department, King Abdul-Aziz University, Jedah (KSA) for doing SEM experiments.

References

[1] V.V. Boldyrev, M. Bulens, B. Delmon, The Control of the Reactivity of Solids, Elseveir, Amsterdam, 1979.
[2] D. Dollimore, Thermochim. Acta 117 (1987) 331.
[3] A. Coetzee, M.E. Brown, D.J. Eve, C.A. Strydom, J. Therm. Anal. 41 (1994) 357.
[4] W.M. Shahheen, M.M. Selim, Thermochim. Acta 322 (1998) 117.
[5] Pospisil, Thermochim. Acta 119 (1987) 261.
[6] Mucka, J. Pavek, Z. Phys. Chem. 131 (1982) 217.
[7] S. Giullermo, M. Arturo, V. Osvaldo, C. Francisco, C. Gerardo, Thin Solid Films 373 (2000) 235.
[8] A. Coetzee, D.J. Eve, M.E. Brown, J. Therm. Anal. 39 (1993) 947.
[9] M.A. Gabal, Thermochim. Acta 402 (2003) 199.
[10] L.H. Tagle, F.R. Diaz, L. Rivera, Thermochim. Acta 118 (1987) 111.
[11] International Center for Diffraction Data, JCPDS, PDF2 Data Base Swarthmore, PA, USA, 1996.
[12] El-H.M. Diefallah, Thermochim. Acta 202 (1992) 1.
[13] El-H.M. Diefallah, A.Y. Obaid, A.H. Qusti, A.A. El-Bellihi, M.A. Abdel Wahab, M.M. Moustafa, Thermochim. Acta 274 (1996) 165.
[14] A.W. Coats, J.P. Redfern, Nature 20 (1964) 68.
[15] T. Ozawa, Bull. Chem. Soc. Jpn. 38 (1965) 1881.
[16] K. Nagase, K. Sato, N. Tanaka, Bull. Chem. Soc. Jpn. 48 (1975) 439.
[17] J.A. Dean, Lange's Hand Book of Chemistry, 12th ed., McGraw-Hill, New York, 1979.
[18] D. Dollimore, D.L. Griffths, J. Therm. Anal. 2 (1970) 229.
[19] D. Dollimore, D.L. Griffths, D. Nicholson, J. Chem. Soc. (1963) 2617.
[20] J.D. Danforth, J. Dix, J. Am. Chem. Soc. 93 (1971) 6843.
[21] K. Nagase, Bull. Chem. Soc. Jpn. 45 (1972) 2166.
[22] El-H.M. Diefallah, M.A. Gabal, A.A. El-Bellihi, N.A. Eissa, Thermochim. Acta 376 (2001) 43.
[23] El-H.M. Diefallah, M.A. Mousa, A.A. El-Bellihi, E.H. El-Mossalamy, G.A. El-Sayed, M.A. Gabal, J. Anal. Appl. Pyrl. 62 (2002) 205.